Once you have Acrobat Reader open on your computer, click on the Comment tab at the right of the toolbar:

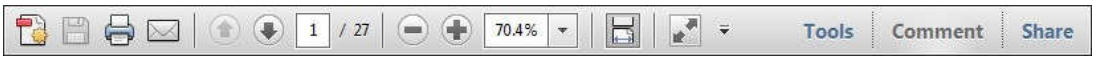

This will open up a panel down the right side of the document. The majority of tools you will use for annotating your proof will be in the Annotations section, pictured opposite. We've picked out some of these tools below:

1. Replace (Ins) Tool – for replacing text.

Strikes a line through text and opens up a text box where replacement text can be entered.

How to use it

- Highlight a word or sentence.
- Click on the Replace (Ins) icon in the Annotations section.
- Type the replacement text into the blue box that appears.

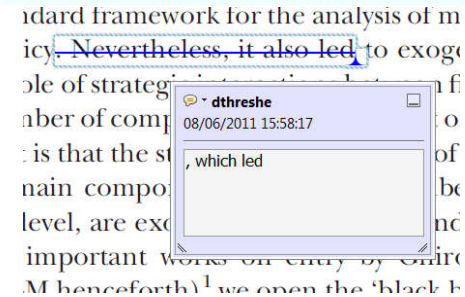

2. Strikethrough (Del) Tool – for deleting text.

Strikes a red line through text that is to be deleted.

How to use it

- Highlight a word or sentence.
- Click on the Strikethrough (Del) icon in the Annotations section.

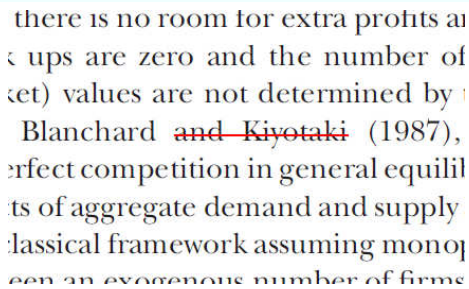

3. Add note to text Tool – for highlighting a section to be changed to bold or italic.

Highlights text in yellow and opens up a text box where comments can be entered.

How to use it

- Highlight the relevant section of text.
- Click on the Add note to text icon in the Annotations section.
- Type instruction on what should be changed regarding the text into the yellow box that appears.

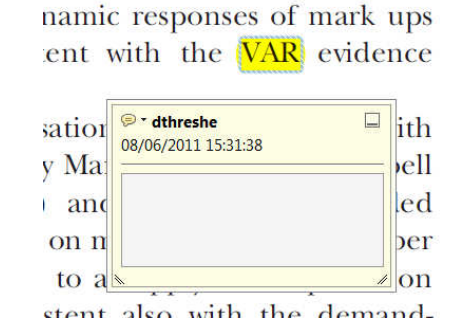

4. Add sticky note Tool – for making notes at specific points in the text.

Marks a point in the proof where a comment needs to be highlighted.

How to use it

- Click on the Add sticky note icon in the Annotations section.
- Click at the point in the proof where the comment should be inserted.
- Type the comment into the yellow box that appears.

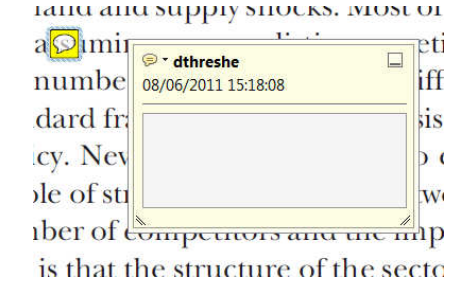

5. Attach File Tool – for inserting large amounts of text or replacement figures.

Inserts an icon linking to the attached file in the appropriate place in the text.

How to use it

- Click on the Attach File icon in the Annotations section.
- Click on the proof to where you'd like the attached file to be linked.
- Select the file to be attached from your computer or network.
- Select the colour and type of icon that will appear in the proof. Click OK.

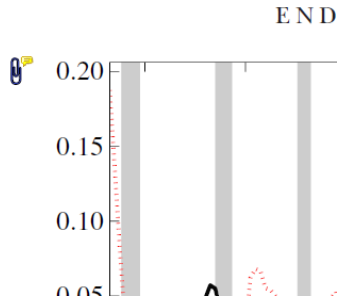

6. Drawing Markups Tools – for drawing shapes, lines and freeform annotations on proofs and commenting on these marks.

Allows shapes, lines and freeform annotations to be drawn on proofs and for comment to be made on these marks.

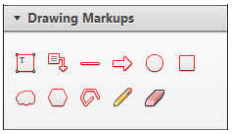

How to use it

- Click on one of the shapes in the Drawing Markups section.
- Click on the proof at the relevant point and draw the selected shape with the cursor.
- To add a comment to the drawn shape, move the cursor over the shape until an arrowhead appears.
- Double click on the shape and type any text in the red box that appears.

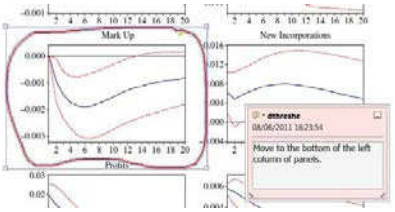

journal

J. Am. Ceram. Soc., 1–6 (2014)
DOI: 10.1111/jace.13408

X-ray Absorption Spectroscopy Studies of the Room-Temperature Ferromagnetic Fe-Doped 6H–$BaTiO_3$

Iuliia Mikulska,[‡] Matjaž Valant,[‡,†] Iztok Arčon,[‡,§] and Darja Lisjak[¶]

[‡]University of Nova Gorica, Nova Gorica SI-5000, Slovenia

[§]Jožef Stefan Institute, Ljubljana SI-1000, Slovenia

[¶]Advanced Materials Department, Jožef Stefan Institute, Ljubljana SI-1000, Slovenia

JACE Journal Code 13408 Manuscript No. | Wiley | Dispatch: 10.12.14 No. of pages: 6 | CE: Muthu malliga PE: Raghu

We investigated the effect of annealing temperature on magnetic properties of 2% and 10% Fe-doped $BaTiO_3$. To understand the possible structural differences between samples treated at different annealing temperatures, and to correlate them with the magnetic properties, several characterization techniques, such as X-ray diffraction and X-ray absorption spectroscopic methods (XANES and EXAFS) were employed. We found that the 2% Fe-doped $BaTiO_3$ pseudocubic perovskite is paramagnetic regardless of the heat-treatment conditions. Initially paramagnetic 10% Fe-doped 6H–$BaTiO_3$, treated at 1250°C, became ferromagnetic after additional annealing at higher temperature. We have crystalographically characterized the cation ordering processes in the 6H–$BaTiO_3$ that occurred during the high-temperature annealing. The ferromagnetism that is induced in this stage is most probably associated with the observed diffusion processes but it extrinsic character still cannot be fully disregarded.

I. Introduction

Simultaneous presence of semiconducting and ferromagnetic properties makes dilute magnetic oxide (DMO) materials attractive for application in spintronic and magnetoelectronic devices.[1–3] The room-temperature magnetism in the wide bandgap semiconductors would be of the immense technological importance only if the magnetic coupling is of intrinsic character and not a consequence of paramagnetic dopant segregation or any other extrinsic reason.

Some of the investigated DMO candidates possess room-temperature ferromagnetism when doped with a small percentage of transition metal ions, for example, Mn-doped ZnO,[4] Fe-doped SnO_2.[5] Even for these well investigated systems still some disputes over the intrinsic nature of the magnetism exists.[6,7] Another very promising DMO material is Fe-doped $BaTiO_3$. Due to the observed room-temperature magnetism it is very intensively investigated material in a wide range of dopant concentration.[8–20]

However, the reports on the properties of this material are extremely controversial. The first source of this controversy is in the phase transition that occurs with Fe doping and is often not properly considered. It is known that tetragonal perovskite $BaTiO_3$ can accommodate about 1% of Fe^{3+} on the perovskite B site.[13,21] Depending on the synthesis conditions from 6% to 13% of Fe is required to fully stabilize the hexagonal 6H–$BaTiO_3$ structure.[17,21–23] The intermediate dopant concentrations yield two phase mixture.[13,21] However, the literature reports claim the intrinsic room-temperature magnetism for the dopant levels from 2% to 10%, although no $BaTiO_3$ phase in its bulk form can contain such Fe concentration. Of course, with the increase in the nominal Fe concentration toward 10%, the saturation magnetization of the biphasic mixture increases as the amount of the paramagnetic phase reduces. It would also be expected that an increase in the Fe content in Fe-doped 6H–$BaTiO_3$ phase would enhance the magnetic ordering. Interestingly, it has been shown the opposite: the saturation magnetization of the low end-member with 10% of Fe is the highest while any increase in Fe content causes a gradual decrease in the magnetism until the material becomes paramagnetic at doping level of 70%.[11,13]

Despite intensive research and a number of reports that claim the room-temperature ferromagnetism in Fe-doped $BaTiO_3$ the origin of the magnetic coupling still remains unknown.[10–13,17,21,24] Some authors claim that the room-temperature ferromagnetism is attributed to some structural characteristics, such as ordering of oxygen vacancies[8] or Fe pairing on Ti(2) sites[12,25] whereas others attribute the ferromagnetic behavior to the double exchange interaction, due to the simultaneous presence of Fe^{3+} and Fe^{2+} or Fe^{4+} valance states.[15,16,23] Also, there are assumptions that Ti^{4+} partially reduces to Ti^{3+}, which can contribute to the ferromagnetic coupling.[8] In our previous study[26] on 20% Fe-doped 6H–$BaTiO_3$ we showed that Fe^{3+} ions undergo an ordering process with a prolonged high-temperature annealing, which plays a crucial role in induction of the magnetic coupling. We showed that the same batch can be paramagnetic or exhibit some ferromagnetic coupling depending on the degree of the cation ordering. We have described the atomistic mechanism of the ordering and identified the driving force of the ordering to be in reduction in electrostatic repulsion on the Ti(2) sites.

In the light of the newly discovered diffusion processes in Fe-doped 6H–$BaTiO_3$, which are of crucial importance for its functional properties,[25,26] we also decided to thoroughly investigate the low-concentration range of this system, that is, the range of ≤10%. First, we made a clear distinction between properties of the Fe-doped paramagnetic tetragonal $BaTiO_3$ and 6H–$BaTiO_3$ phases. We performed a microscopic structural analysis on the 6H low end-member, 10% Fe-doped 6H-$BaTiO_3$, with intention to understand the possible structural differences between samples treated at different annealing temperatures. We correlated this to magnetic properties and to the similar diffusion processes in highly doped Fe-doped 6H–$BaTiO_3$ to fully describe the crystal chemistry of the entire concentration range that is interesting for the DMO applications.

A. Belik—contributing editor

Manuscript No. 35454. Received August 12, 2014; revised November 21, 2014; approved November 24, 2014.

[†]Author to whom correspondence should be addressed. e-mail: matjaz.valant@ung.si

Here, we have described the ordering processes which are crucial for the establishing of the long-range ferromagnetic coupling in Fe-doped 6H–$BaTiO_3$. Our convincing experimental results bring us closer to understanding the origin of magnetic coupling in this system.

II. Experimental Procedure

Fe-doped $BaTiO_3$ samples with nominal composition of $BaTi_{1-x}Fe_xO_{3-\delta}$ (x = 0.02, 0.1) were synthesized by conventional solid-state reaction method by stoichiometric mixing of raw oxide materials of Fe_2O_3, TiO_2, and $BaCO_3$. Before each heat treatment, the samples were mixed by grinding in planetary mill at 200 rpm for 1 h in ethanol ambient, dried at 70°C and pressed into 3–4 g pellets. First, the pellets were calcined at 1000°C for 5 h. Then, 2% Fe-doped $BaTiO_3$ was treated at 1200°C for 5 h, whereas 10% Fe-doped $BaTiO_3$ was fired twice at 1250°C for 5 h. After this synthesis step, the obtained powders were divided into two parts. One of these parts was additionally annealed at 1400°C for 5 h for 2% Fe-doped $BaTiO_3$, and at 1500°C for 10 h for 10% Fe-doped $BaTiO_3$. All heat treatments were carried out in oxygen atmosphere.

The crystal structure of the samples was analyzed by X-Ray diffractometry (~~PANalytical X'PRO~~). The XRD patterns were performed in reflection (Bragg–Brentano) mode using CuK_α radiation. Data were collected in the range 15°–2θ ≤ 90° with the scan step of 0.008° and with scan step time of 25 s.

The Fe K-edge X-ray absorption spectroscopy (XAS) spectra were collected at the beamline C of HASYLAB at DESY in Hamburg (Germany) simultaneously in fluorescence and transmission detection modes. Ti K-edge XANES spectra were measured at the XAFS beamline of the ELETTRA synchrotron radiation facility in Trieste (Italy) in transmission detection mode. All experimental details are described in our previous study.[26] The Fe and Ti XAS spectra were analyzed with the IFEFFIT program package.[27] Magnetization was measured as function of applied magnetic field on vibrating sample magnetometer (VSM, LakeShore, 7404) at room temperature.

III. Results and Discussion

The crystal structure of the samples was analyzed by XRD. 2% Fe-doped $BaTiO_3$ sample treated at 1200°C has tetragonal crystal structure (space group $P4mm$) with possible traces of hexagonal phase (space group $P63/mmc$) (Fig. 1). The XRD pattern of 2% Fe-doped $BaTiO_3$ additionally annealed at 1400°C for 5 h indicates the presence of mixture of hexagonal and tetragonal phases. In addition to prevailing 6H phase the sample with 10% of Fe treated at 1250°C contains minor amount of the tetragonal perovskite phase. The sample additionally annealed at 1500°C shows a single-phase composition with only 6H–$BaTiO_3$ phase. Our results confirm the main claims of other authors[8,13,21] that the solid solubility limit of Fe in the tetragonal $BaTiO_3$ is below 2 at.%, whereas about 10 at.% of Fe is required to fully stabilize 6H–$BaTiO_3$. In addition, it can be concluded that the low-end stability range of Fe-doped 6H–$BaTiO_3$ is temperature dependent: more than 10% of Fe are needed for stabilization of the structure at 1250°C and below 10% at higher temperature of 1500°C.

First, we have measured the magnetic properties of the tetragonal perovskite phase with the highest possible Fe concentration (i.e., 2%). Regardless the thermal treatment conditions, the paramagnetic behavior has been determined. Magnetization at room temperature as a function of applied magnetic field is shown on Fig. 2.

As the tetragonal perovskite phase is paramagnetic the magnetic properties of the two-phase region between 2% and

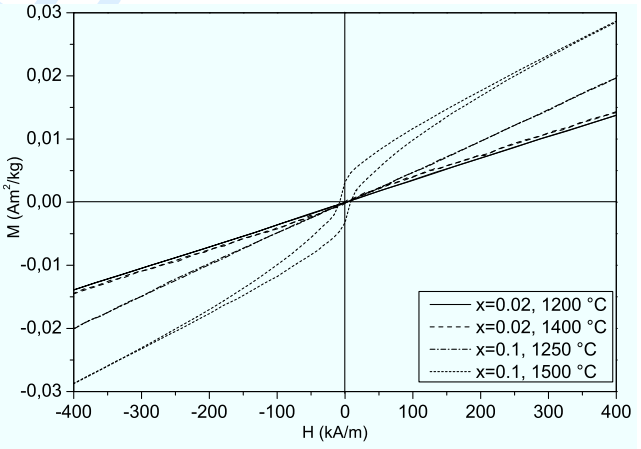

Fig. 2. Room-temperature M(H) loops for 2% and 10% Fe-doped $BaTiO_3$ samples treated at different annealing temperatures.

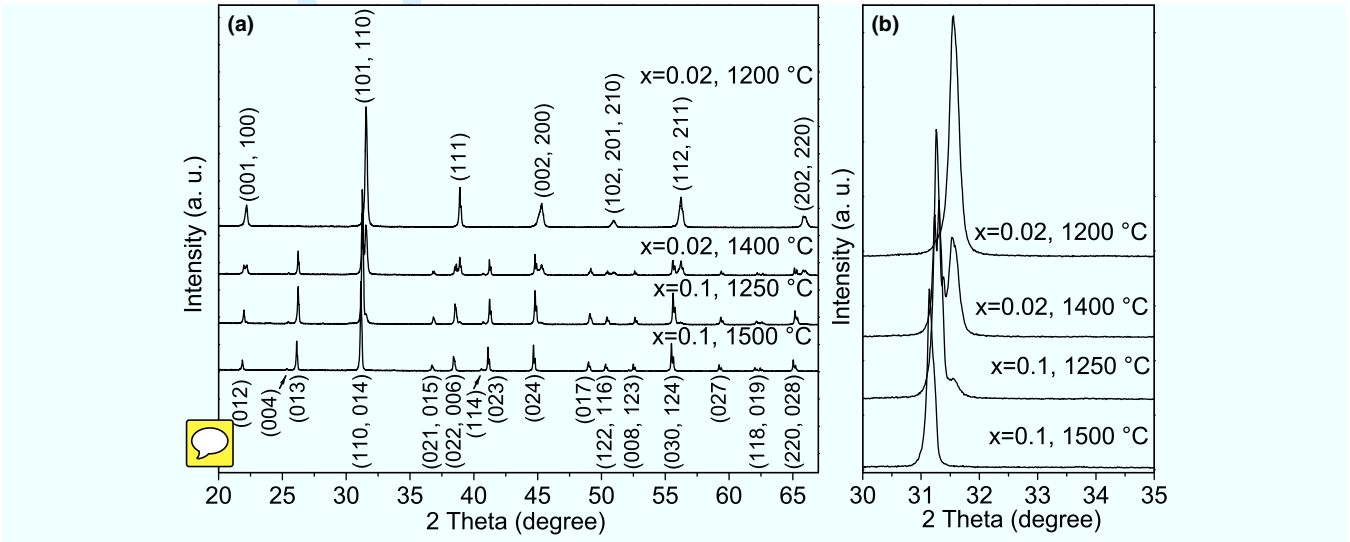

Fig. 1. (a) X-ray diffraction patterns of $BaTi_{1-x}Fe_xO_3$ powder samples treated at different annealing temperatures. The peaks of tetragonal (top) and hexagonal (bottom) $BaTiO_3$ are labeled with Miller indices (hkl). (b) Magnification of diffraction peaks in the 2θ interval 30°–34°, which shows the effect of annealing temperature on the phase evolution of Fe-doped $BaTiO_3$.

10% of Fe are dominated by the ferromagnetic properties of the 6H phase; therefore, this region has not been of our main interest. We analyzed the sample with 10% of Fe that was treated at 1250°C, which has predominant 6H–$BaTiO_3$ phase with a miniscule amount of the paramagnetic tetragonal phase. The sample exhibits pure paramagnetic behavior, so we can conclude that the dominating 6H matrix phase is also paramagnetic. The same sample was additionally annealed at 1500°C and the magnetic measurements showed that this stage of the thermal treatment has induced the ferromagnetic behavior (Fig. 2). Despite the hysteretic behavior the magnetization increases linearly with the increasing magnetic field above 50 kA/m, indicating that ferromagnetic and paramagnetic phases coexist in the sample.

To correlate the observed variation in the magnetic properties with microscopic processes at atomic level, that occur in the 10% Fe-doped 6H–$BaTiO_3$ during thermal treatment, we performed a detailed analysis of Fe valence state and local structure around Fe cations in the crystal structure by Fe K-edge XANES and EXAFS.

To verify the possible changes in the valance state of the Fe cations in the 10% Fe-doped 6H–$BaTiO_3$ samples we analyzed Fe K-edge XANES spectra (Fig. 3). A decrease in the oxidation state of the absorbing atom shifts the energy position of the absorption edge to the lower energies. A shift of about 4.5 eV is observed between Fe^{3+} and Fe^{2+} in reference compounds with well-established Fe valance states (Fe^{3+} in Fe_2O_3 and $NdFeO_3$, and Fe^{2+} in $FeSO_4$), in agreement with previous observations.[28,29] XANES spectra of

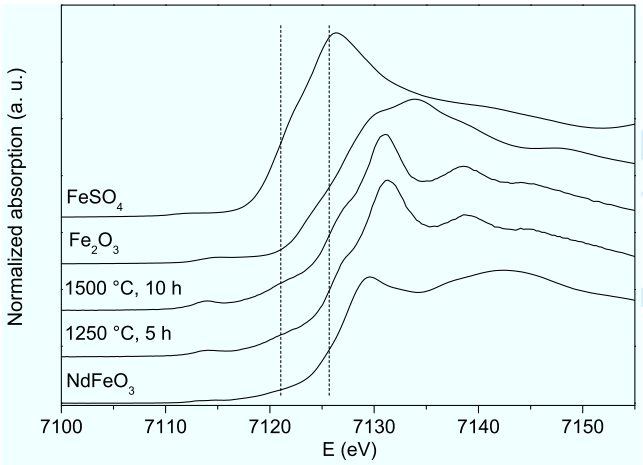

Fig. 3. Normalized Fe K-edge XANES spectra measured on the 10% Fe-doped 6H–$BaTiO_3$ samples after the different heat treatments and reference compounds [$Fe(III)_2O_3$, $NdFe(III)O_3$, and $Fe(II)SO_4$] with known Fe valance state. Two vertical lines are plotted at the position of the Fe(II) K-edge (7121 eV) and Fe(III) K-edge (7125.7 eV) for comparison of the Fe K-edge positions.

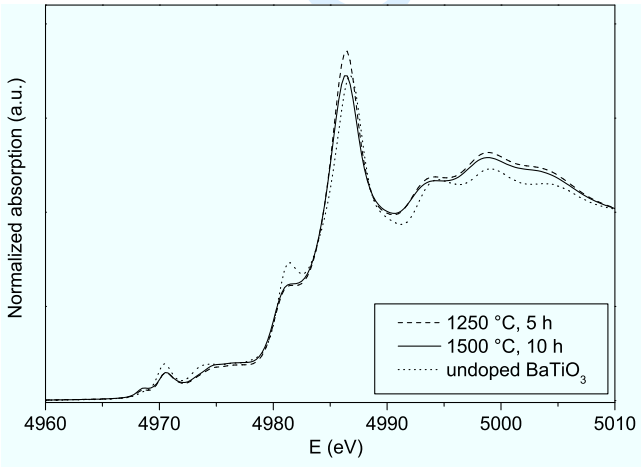

Fig. 4. Normalized Ti K-edge XANES spectra measured on 10% Fe-doped 6H–$BaTiO_3$ powder samples, treated at different annealing temperatures (1250°C and 1500°C), and undoped $BaTiO_3$ with tetragonal (space group *P*4*mm*) crystal structure as a standard for Ti^{4+}.

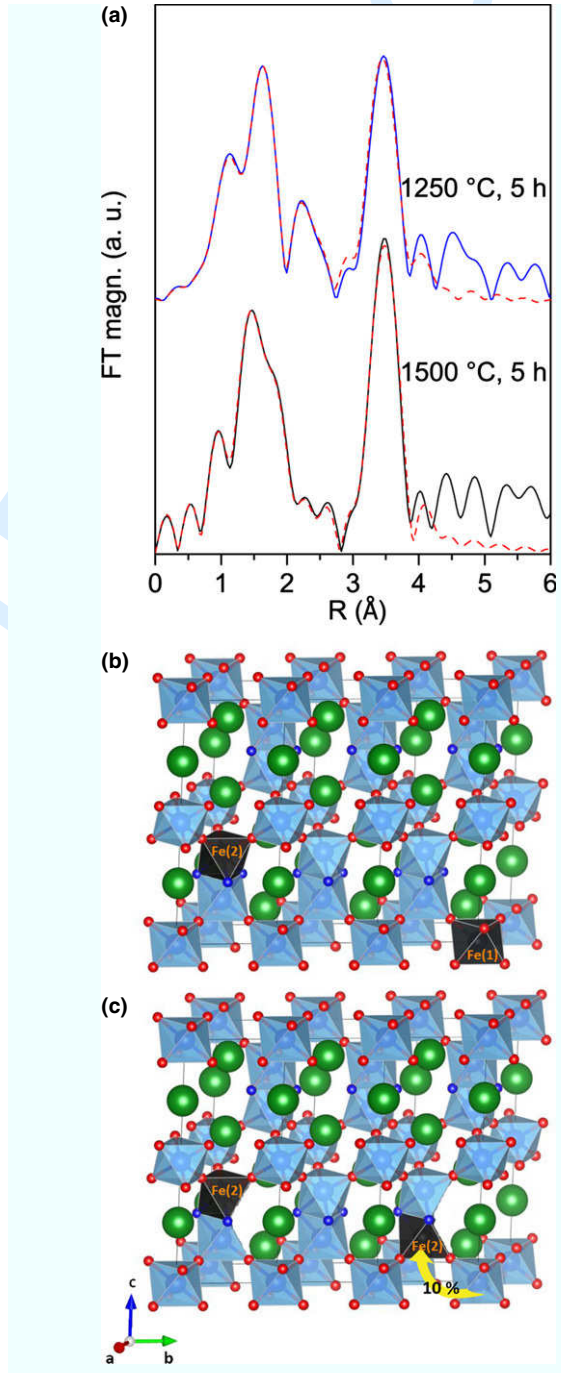

Fig. 5. (a) The Fourier-transform magnitudes of 10% Fe-doped $BaTiO_3$ annealed at different temperatures (dashed line – best fit EXAFS model). (b) and (c) Schematic view of the Fe-distribution within three unit cells of the Fe-doped 6H–$BaTiO_3$ crystal structure (space group *P*63/*mmc*): (b) after treatment at 1250°C for 5 h, (c) additionally annealed at 1500°C for 10 h. The polyhedra represent octahedrally coordinated Ti atoms. The Fe atoms incorporated onto Ti(1) and Ti(2) sites and their coordination octahedra are marked black. The octahedra with missing faces illustrate the oxygen vacancy in the corresponding face-sharing plane. The big spheres are Ba atoms. The dark and light smaller spheres are oxygen atoms on the O(2) and O(1) crystallographic sites, respectively. The arrow marks the movements of Fe^{3+} from Ti(1) sites to Ti(2) sites after additional annealing at 1500°C for 10 h.

Colour online, B&W in print

both samples exhibit similar shape and the same energy position of Fe K-edge and preedge resonances. Small differences in the edge profile and intensity of the preedge resonances can be attributed to changes in average local environment of Fe cations, detected in the Fe K-edge EXAFS analysis.[28] Comparison of the Fe K-edge energy positions of the samples and reference compounds reveals that all iron atoms in the samples are in trivalent form.

Comparison of Ti K-edge XANES spectra of the different Fe-doped 6H–$BaTiO_3$ samples shows that spectra are identical (Fig. 4). The Ti K-edge spectrum of the reference undoped tetragonal perovskite $BaTiO_3$, which is a well-established reference for Ti^{4+} valence state, slightly differs in the shape of the edge and preedge features compared with spectra of the two samples, due to the difference in the crystal structures. However, the energy position of the Ti K-edge in the samples coincides well with that in undoped perovskite $BaTiO_3$, so we can conclude that all titanium in the 6H–$BaTiO_3$ samples is in tetravalent state.

We used EXAFS analysis to determine the possible changes in local environment of Fe atoms incorporated onto Ti(1) and Ti(2) crystallographic sites. Ti cations in 6H–$BaTiO_3$ have two different crystallographic sites: Ti(1) and Ti(2) atoms are situated in the corner-sharing and face-sharing octahedra, respectively. On both crystallographic sites Ti cations in 6H–$BaTiO_3$ are octahedrally coordinated, however, they have small, but significant differences in the local surroundings.[26]

The EXAFS signal is a superposition of two signals, one from the Fe(1) atoms located at Ti(1) site and the other, arising from Fe(2) atoms located at Ti(2) site. Contributions of individual shells of atoms around Fe atom are visible up to about 5 Å in Fourier-Transform (FT) magnitudes of representative EXAFS spectra. Fourier Transform (FT) of Fe K-edge EXAFS signals consist of contributions from two Fe coordination shells: first shell is the contribution of the oxygen atoms and one titanium atom, second shell is superimposed contribution of the barium and titanium atoms (Fig. 5). Qualitative EXAFS analysis shows that the local neighborhood of Fe in all samples of Fe-doped $BaTiO_3$ is similar, with small but significant differences in the first and second coordination shells.

The quantitative information on Fe local structure around the Ti(1) and Ti(2), that is, Fe(1) and Fe(2), crystallographic sites was obtained from quantitative EXAFS analysis. EXAFS spectra were modeled with an ab initio FEFF[30] calculation using simultaneous fit of the Fe EXAFS spectra of 10% Fe-doped $BaTiO_3$ sample sintered at 1250°C for 5 h and 10% Fe-doped $BaTiO_3$ sample additionally annealed at 1500°C for 10 h. EXAFS spectra have been fitted using similar model, as in our previous EXAFS study of 20% Fe-doped $BaTiO_3$.[26] Two FEFF models with iron atoms incorporated onto Ti(1) and Ti(2) crystallographic sites were constructed, based on the 6H–$BaTiO_3$ crystal structure with $P63/mmc$ space group (a = 5.7240 Å and c = 13.9650 Å).[31] Measured EXAFS spectra were modeled with a linear combination of both FEFF models, where relative amount of each model signal ($X_{Fe(1)}$and $X_{Fe(2)}$)—representing the occupancy of Fe on each Ti site was allowed to vary in the EXAFS fit. Models include two neighbor shells, comprising all single-scattering and significant multiple-scattering paths with length of up to 4.52 Å. The structure parameters (type and neighbor atoms, distances and Debye–Waller factors) of nearest neighbor shells around Fe incorporated onto Ti(1) and Ti(2) sites in 10% Fe-doped $BaTiO_3$ are listed in the Table I. The fit of the both EXAFS spectra was performed with the background corefinement.[27]

In FEFF models we allow to vary separately the common shift of the energy origin (ΔE_0), occupation probability of Fe in Ti(2) crystallographic site ($X_{Fe(2)}$) the distances and Debye–Waller factors for the first four single-scattering [Fe(1)-O(1/1), Fe(2)-O(2/1), Fe(2)-O(2/2), and Fe(2)-Ti(2/1)] paths. For the rest of the paths the general linear expansion coefficient was allowed to vary to compute distances, whereas correlated Debye model was used to determine the Debye–Waller factors by varying the Debye temperature parameter. In addition, Fe(2)–Ba(2/1), Fe(2)–Ba(2/3), and Fe(1)–Ba(1/2) distances were allowed to vary separately. The site occupation probabilities of Fe in Ti(1) and Ti(2) sites were constrained to a unit sum. The amplitude reduction factor was kept fixed at 0.75, the value determined in the Fe K-edge EXAFS fit of $Li_2Fe_{0.8}Mn_{0.2}SiO_4$ in Ref. [29]. The coordination number of neighboring atoms was kept fixed according to the crystallographic data. According to electroneutrality, substituting Ti^{4+} ions by Fe^{3+} ions leads to formation of oxygen vacancies, which are known to be situated mainly in the phase-sharing plane of the hexagonal crystal structure of Fe-doped $BaTiO_3$ (O(2/2) site).[17,32–35] Thus, to verify the

Table I. Parameters of the Nearest Neighbors Around Fe Atom on Ti(1) and Ti(2) Crystallographic Sites for the 10% Fe-Doped $BaTiO_3$ Samples Treated at Different Annealing Temperatures (1250°C and 1500°C)†

ΔE_0 Fe(2)	1250°C, 5 h 0.7 ± 0.5 (eV) $X_{Fe(2)}$ = 0.51(4)			1500°C, 5 h 0.3 ± 0.5 (eV) $X_{Fe(2)}$ = 0.61(3)		
	N	R (Å)	σ^2 (Å^2)	N	R (Å)	σ^2 (Å^2)
O(2/1)	2.9	1.88 (1)	0.007 (3)	2.9	1.89 (1)	0.002 (1)
O(2/2)	2.9	2.02 (1)	0.004 (2)	1.8 (8)	2.02 (4)	0.004 (2)
Ti(2/1)	1	2.7 (1)	0.003 (1)	0.9	2.59 (2)	0.008 (1)
Fe(2/1)	0	—	—	0.1	2.88 (1)	0.008 (2)
Ba(2/1)	2.9	3.40 (1)	0.005 (1)	2.9	3.31 (1)	0.005 (1)
Ba(2/2)	1	3.50 (1)	0.005 (1)	1	3.45 (1)	0.005 (1)
Ba(2/3)	3	3.57 (1)	0.005 (1)	3	3.51 (1)	0.005 (1)
Ti(2/2)	3	3.94 (1)	0.008 (1)	3	3.88 (1)	0.008 (1)
O(2/3)	3	4.08 (1)	0.016 (1)	3	4.02 (1)	0.016 (1)
Fe(1)	$X_{Fe(1)}$ = 0.49 (4)			$X_{Fe(1)}$ = 0.39 (3)		
O(1/1)	5.8	1.99 (2)	0.010 (2)	5.8	2.04 (1)	0.003 (1)
Ba(1/1)	2	3.49 (1)	0.005 (1)	2	3.44 (1)	0.005 (1)
Ba(1/2)	6	3.65 (1)	0.005 (1)	6	3.70 (1)	0.005 (1)
Ti(1/1)	6	3.94 (1)	0.008 (1)	6	3.88 (2)	0.008 (1)
O(1/2)	12	4.52 (1)	0.016 (1)	12	4.45 (1)	0.016 (1)
O(1/3)	12	4.53 (1)	0.016 (1)	12	4.46 (1)	0.016 (1)

†The neighbor atom annotations are based on Fe atoms at two crystallographic sites [Ti(1) and Ti(2)] and Fe neighbor atoms ordered by distance in 6H–$BaTiO_3$ crystal structure: for example, O(2/1) are oxygen neighbors of Fe(2) atoms located at 1.96 Å; O(2/2) are oxygen neighbors of Fe(2) atoms located at 1.99 Å.

N, number of neighbor atoms; R, distance from the Fe atom; σ^2, Debye–Waller factor.

aforementioned statement the O(2/2) coordination number was allowed to vary separately. Also, the coordination number of the Fe(2/1) atoms was varied in purpose to verify the formation of Fe pairs in the Ti_2O_9 polyhedra (i.e., Fe_2O_9). For Fe(2)–Fe(2/1) and Fe(2)–Ti(2/1) paths the same Debye–Waller factor was used. Fe(2)–Fe(2/1) distance was allowed to very separately. Simultaneous fit of the two EXAFS spectra was carried out with intent to stabilize the fit by increasing the number of independent points and decreasing the number of variables. Thus, to minimize number of variables some of the parameters in the simultaneous relaxation were constrained to the common values for the two samples, in particular, Debye–Waller factor for Fe(2)–O(2/2) path and Fe(2)–Ba(2/1) distance and Debye temperature parameter.

A very good agreement between the model and the experimental spectrum of 10% Fe-doped $BaTiO_3$ was found in the R-range from 1.1 to 3.9 Å and in the k-interval 4.3–12 $Å^{-1}$ using k^2-weight for sample treated at 1250°C and k^3-weight for sample additionally annealed at 1500°C.

A unit cell of 6H–$BaTiO_3$ contains six octahedrally coordinated Ti^{4+} ions: two at Ti(1) and four at Ti(2) sites. Therefore, in a case of random distribution 2/3 of Fe ions occupy Ti(2) sites, whereas other 1/3 occupy Ti(1) crystallographic sites. In our case, quantitative EXAFS analysis reveals that after heat treatment at 1250°C about half of all Fe atoms preferably occupy the Ti(1) crystallographic sites, whereas the other half of Fe atoms occupy Ti(2) site (Fig. 5). For sample fired at 1250°C for 5 h the number of oxygen vacancies in O(2/2) crystallographic site was below detection limit, so the coordination number of O(2/2) atoms was fixed to 2.94, value, which corresponds to the random distribution of oxygen vacancies around Fe(2) in the sample. No formation of Fe pairs has been detected (Table I). For the neighboring atoms we did not find significant distortion, except a slight relaxation of interatomic distances.

After additional annealing at 1500°C about 10% of iron atoms redistributed from Ti(1) ($X_{Fe(1)}$ = 40%) to Ti(2) ($X_{Fe(1)}$ = 60%) site. The redistribution is most probably driven by the same driving force as established in Ref. [26]: reduction in electrostatic repulsion within Ti_2O_9 face-sharing octahedral. In contrast to 20% Fe-doped $BaTiO_3$, during the fit procedure the number of Fe(2)–Fe(2/1) pairs in 10% Fe-doped $BaTiO_3$ sample could not be reliably determined by varying the coordination number of the Fe(2/1) neighbor atoms. However, it was found that fixing the coordination number of the Fe(2/1) neighbor atoms to the 0.1 improves the fit. For this sample ordering of the oxygen vacancies by varying the coordination number of the O(2/2) atoms was detected.

Our studies show that very subtle differences exist in the cation ordering processes of different Fe-doped 6H–$BaTiO_3$ samples. Despite these differences the ordering process is always associated with induction of the room-temperature ferromagnetism. Based on our analysis, the ferromagnetism appears independently from existence of the Fe–Fe pairs or the oxygen vacancy segregation at O(2/2) site. These two crystallographic features are most frequently considered as an origin of the magnetic coupling in this system. Here, we showed that in the ferromagnetic 10% Fe-doped 6H–$BaTiO_3$ no significant formation of Fe–Fe pairs exists while previously[26] has already been shown that the ferromagnetism can also exist without the segregation of oxygen vacancies in O(2/2) site. However, it has been undoubtedly seen that the induction of the ferromagnetism is in some way associated with the high-temperature annealing and most probably with the observed diffusion processes but it extrinsic character still cannot be fully disregarded.

IV. Conclusions

2% and 10% Fe-doped $BaTiO_3$ samples were synthesized by the solid-state reaction method at different annealing temperatures. The 2%-doped $BaTiO_3$ samples were found to be paramagnetic at RT after both annealing temperatures. The 10% Fe-doped $BaTiO_3$ sample treated at 1250°C is paramagnetic, whereas 10% Fe-doped $BaTiO_3$ sample additionally annealed at 1500°C exhibited ferromagnetic behavior. Fe and Ti K-edge XANES analysis showed no variations in the valance state of Fe^{3+} and Ti^{4+} cations in all 10% Fe-doped $BaTiO_3$ samples. A Fe K-edge EXAFS analysis of the 10% Fe-doped $BaTiO_3$ sample treated at 1250°C revealed that Fe^{3+} ions preferably occupied the Ti(1) sites. At this synthesis step no preferential distribution of oxygen vacancies has been detected. During the additional annealing at 1500°C for 10 h a redistribution of the Fe cations from the Ti(1) sites to Ti(2) sites was detected, resulting in a random distribution of the Fe cations over these sites. Such redistribution was accompanied by segregation of oxygen vacancies on the O(2/2) site. The induction of the ferromagnetism coincides with the appearance of the observed diffusion processes. However, none of the diffusion processes can be undoubtedly identified as the one that induces the ferromagnetic spin coupling.

Acknowledgments

This work has been supported by the Slovenian Research Agency Research Programmes P1-0112, P2-0377, and PR-04988, project N2-0005, DESY and the European Community's FP7 Programme (FP7/2007-2013) under grant agreement CALIPSO n_312284 (EU Support of Access to Synchrotrons/FELs in Europe). Access to synchrotron radiation facilities of HASYLAB (project I-20110082 EC) and ELETTRA (project 20110127) is acknowledged. We thank Roman Chernikov and Edmund Welter of HASYLAB and Giuliana Aquilanti of ELETTRA for expert advice on beamline operation. The CENN Nanocenter is acknowledged for the usage of the VSM.

References

[1] J. M. D. Coey, "Dilute Magnetic Oxides," *Curr. Opin. Solid St M*, **10** [2] 83–92 (2006).
[2] S. A. Chambers, T. C. Droubay, C. M. Wang, K. M. Rosso, S. M. Heald, D. A. SchwartZ, K. R. Kittilstved, and D. R. Gamelin, "Ferromagnetism in Oxide Semiconductors," *Mater. Today*, **9** [11] 28–35 (2006).
[3] T. Dietl, "A Ten-Year Perspective on Dilute Magnetic Semiconductors and Oxides," *Nat. Mater.*, **9** [12] 965–74 (2010).
[4] P. Sharma, A. Gupta, K. V. Rao, F. J. Owens, R. Sharma, R. Ahuja, J. M. O. Guillen, B. Johansson, and G. A. Gehring, "Ferromagnetism Above Room Temperature in Bulk and Transparent Thin Films of Mn-Doped ZnO," *Nat. Mater.*, **2** [10] 673–7 (2003).
[5] A. Punnoose, J. Hays, A. Thurber, M. H. Engelhard, R. K. Kukkadapu, C. Wang, V. Shutthanandan, and S. Thevuthasan, "Development of High-Temperature Ferromagnetism in SnO_2 and Paramagnetism in SnO by Fe Doping," *Phys. Rev. B*, **72** [5] ???–??? (2005). 4
[6] D. C. Kundaliya, S. B. Ogale, S. E. Lofland, S. Dhar, C. J. Metting, S. R. Shinde, Z. Ma, B. Varughese, K. V. Ramanujachary, L. Salamanca-Riba, and T. Venkatesan, "On the Origin of High-Temperature Ferromagnetism in the Low-Temperature-Processed Mn-Zn-O System," *Nat. Mater.*, **3** [10] 709–14 (2004).
[7] R. Adhikari, A. K. Das, D. Karmakar, T. V. C. Rao, and J. Ghatak, "Structure and Magnetism of Fe-Doped SnO(2) Nanoparticles," *Phys. Rev. B*, **78** [2] ???–??? (2008). 5
[8] X. K. Wei, T. Zou, F. Wang, Q. H. Zhang, Y. Sun, L. Gu, A. Hirata, M. W. Chen, Y. Yao, C. Q. Jin, and R. C. Yu, "Origin of Ferromagnetism and Oxygen-Vacancy Ordering Induced Cross-Controlled Magnetoelectric Effects at Room Temperature," *J. Appl. Phys.*, **111** [7] ???–??? (2012). 6
[9] J. J. Wei, N. Zhang, J. F. Fan, X. M. Yin, and H. X. Cao, "Magnetoelectric Effect in Bilayer Composites of Fe-Doped BaTiO(3) and Terfenol-D," *J. Phys.-Condensed Matter*, **20** [8] ???–??? (2008). 7
[10] X. K. Wei, Y. T. Su, Y. Sui, Q. H. Zhang, Y. Yao, C. Q. Jin, and R. C. Yu, "Structure, Electrical and Magnetic Property Investigations on Dense Fe-Doped Hexagonal $BaTiO_3$," *J. Appl. Phys.*, **110** [11] ???–??? (2011). 8
[11] X. K. Wei, L. D. Yao, X. Shen, Y. Yang, S. J. You, F. Y. Li, C. Q. Jin, and R. C. Yu, "Structural Modulation and Magnetic Properties of Hexagonal $Ba(Ti_{1-X}Fe_x)O_3$-Delta Ceramics," *Phys. B*, **405** [23] 4851–4 (2010).
[12] S. Ray, P. Mahadevan, S. Mandal, S. R. Krishnakumar, C. S. Kuroda, T. Sasaki, T. Taniyama, and M. Itoh, "High Temperature Ferromagnetism in Single Crystalline Dilute Fe-Doped BaTiO(3)," *Phys. Rev. B*, **77** [10] ???–??? (2008). 9
[13] N. V. Dang, T. D. Thanh, L. V. Hong, V. D. Lam, and T. L. Phan, "Structural, Optical and Magnetic Properties of Polycrystalline $BaTi_{1-X}Fe_xO_3$ Ceramics," *J. Appl. Phys.*, **110** [4] ???–??? (2011). 10
[14] G. Radaelli, D. Petti, E. Plekhanov, I. Fina, P. Torelli, B. R. Salles, M. Cantoni, C. Rinaldi, D. Gutiérrez, G. Panaccione, M. Varela, S. Picozzi, J. Fontcuberta, and R. Bertacco, "Electric Control of Magnetism at the Fe/$BaTiO_3$ Interface," *Nat. Commun.*, **5**, ???–??? (2014). 11

[15]Z. G. Guo, L. H. Yang, H. M. Qiu, X. D. Zhan, J. H. Yin, and L. P. Cao, "Structural, Magnetic and Dielectric Properties of Fe-Doped $BaTiO_3$ Solids," *Mod. Phys. Lett. B*, **26** [9] ???–??? (2012).

[16]F. T. Lin, D. M. Jiang, X. M. Ma, and W. Z. Shi, "Effect of Annealing Atmosphere on Magnetism for Fe-Doped $BaTiO_3$ Ceramic," *Phys. B*, **403** [17] 2525–9 (2008).

[17]F. T. Lin, D. M. Jiang, X. M. Ma, and W. Z. Shi, "Influence of Doping Concentration on Room-Temperature Ferromagnetism for Fe-Doped $BaTiO_3$ Ceramics," *J. Magn. Magn. Mater.*, **320** [5] 691–4 (2008).

[18]F. T. Lin and W. Z. Shi, "Effects of Doping Site and Pre-Sintering Time on Microstructure and Magnetic Properties of Fe-Doped $BaTiO_3$ Ceramics," *Phys. B*, **407** [3] 451–6 (2012).

[19]F. T. Lin and W. Z. Shi, "Influence of Non-Isovalent Ion Substitution at A Site on Microstructure and Magnetic Properties of $Ba(Ti_{0.3}Fe_{0.7})O$-3 Ceramic," *J. Alloy. Compd.*, **495** [1] 167–72 (2010).

[20]A. Rajamani, G. F. Dionne, D. Bono, and C. A. Ross, "Faraday Rotation, Ferromagnetism, and Optical Properties in Fe-Doped $BaTiO_3$," *J. Appl. Phys.*, **98** [6] ???–??? (2005).

[21]S. Y. Qiu, W. Li, Y. Liu, G. H. Liu, Y. Q. Wu, and N. Chen, "Phase Evolution and Room Temperature Ferroelectric and Magnetic Properties of Fe-Doped $BaTiO_3$ Ceramics," *Trans. Nonferrous Metals Soc. China*, **20** [10] 1911–5 (2010).

[22]T. A. Vanderah, J. M. Loezos, and R. S. Roth, "Magnetic Dielectric Oxides: Subsolidus Phase Relations in the $BaO:Fe_2O_3:TiO_2$ System," *J. Solid State Chem.*, **121** [1] 38–50 (1996).

[23]H. M. Nguyen, N. V. Dang, P. Y. Chuang, T. D. Thanh, C. W. Hu, T. Y. Chen, V. D. Lam, C. H. Lee, and L. V. Hong, "Tetragonal and Hexagonal Polymorphs of $BaTi_{1-X}Fe_xO_3$-Delta Multiferroics Using X-ray and Raman Analyses," *Appl. Phys. Lett.*, **99** [20] ???–??? (2011).

[24]T. Chakraborty, S. Ray, and M. Itoh, "Defect-Induced Magnetism: Test of Dilute Magnetism in Fe-Doped Hexagonal $BaTiO_3$ Single Crystals," *Phys. Rev. B*, **83** [14] ???–??? (2011).

[25]T. Chakraborty, C. Meneghini, G. Aquilanti, and S. Ray, "Microscopic Distribution of Metal Dopants and Anion Vacancies in Fe-Doped $BaTiO_3$-Delta Single Crystals," *J. Phys.-Condensed Matter*, **25** [23] ???–??? (2013).

[26]M. Valant, I. Arčon, I. Mikulska, and D. Lisjak, "Cation Order–Disorder Transition in Fe-Doped 6H-$BaTiO_3$ for Dilute Room-Temperature Ferromagnetism," *Chem. Mater.*, **25** [17] 3544–50 (2013).

[27]B. Ravel and M. Newville, "Athena, Artemis, Hephaestus: Data Analysis for X-ray Absorption Spectroscopy Using IFEFFIT," *J. Synchrotron Radiat.*, **12**, 537–41 (2005).

[28]I. Arcon, J. Kolar, A. Kodre, D. Hanzel, and M. Strlic, "XANES Analysis of Fe Valence in Iron Gall Inks," *X-Ray Spectrom.*, **36** [3] 199–205 (2007).

[29]R. Dominko, C. Sirisopanaporn, C. Masquelier, D. Hanzel, I. Arcon, and M. Gaberscek, "On the Origin of the Electrochemical Capacity of $Li_2Fe_{0.8}Mn_{0.2}SiO_4$," *J. Electrochem. Soc.*, **157** [12] A1309–16 (2010).

[30]J. J. Rehr, R. C. Albers, and S. I. Zabinsky, "High-Order Multiple-Scattering Calculations of X-Ray-Absorption Fine-Structure," *Phys. Rev. Lett.*, **69** [23] 3397–400 (1992).

[31]J. Akimoto, Y. Gotoh, and Y. Oosawa, "Refinement of Hexagonal $BaTiO_3$," *Acta Crystallogr. Sec. C*, **50** [2] 160–1 (1994).

[32]I. E. Grey, C. Li, L. M. D. Cranswick, R. S. Roth, and T. A. Vanderah, "Structure Analysis of the 6H–Ba(Ti, Fe^{3+}, Fe^{4+})O^{3-} ΔSolid Solution," *J. Solid State Chem.*, **135** [2] 312–21 (1998).

[33]E. Mashkina, C. McCammon, and F. Seifert, "A Mossbauer Study of Oxygen Vacancy and Cation Distribution in 6H-$BaTi_{1-X}Fe_xO_{3-x/2}$," *J. Solid State Chem.*, **177** [1] 262–7 (2004).

[34]I. E. Grey, L. M. D. Cranswick, and C. Li, "Accurate Site Occupancies for Light Atoms From Powder X-ray Data? Oxygen Vacancy Ordering in 6H-$BaFe_{0.67}Ti_{0.33}O_3$-Delta (Delta = 0.08 and 0.32)," *J. Appl. Crystallogr.*, **31**, 692–9 (1998).

[35]T. A. Colson, M. J. S. Spencer, and I. Yarovsky, "A DFT Study of the Perovskite and Hexagonal Phases of $BaTiO_3$," *Comp. Mater. Sci.*, **34** [2] 157–65 (2005). □

Author Query Form

Journal: JACE
Article: 13408

Dear Author,
During the copy-editing of your paper, the following queries arose. Please respond to these by marking up your proofs with the necessary changes/additions. Please write your answers on the query sheet if there is insufficient space on the page proofs. Please write clearly and follow the conventions shown on the attached corrections sheet. If returning the proof by fax do not write too close to the paper's edge. Please remember that illegible mark-ups may delay publication.
Many thanks for your assistance.

Query reference	Query	Remarks
1	**AUTHOR: As per the journal style, please limit the number of characters up to 30 in short title.**	
2	**AUTHOR: Please check that the title, author names, affiliations, and corresponding author information is listed accurately for publication.**	
3	**AUTHOR: Please give manufacturer information for PANalytical X'PRO: company name, town, state (if USA), and country.**	
4	**AUTHOR: Please provide the page range for reference [5].**	
5	**AUTHOR: Please provide the page range for reference [7].**	
6	**AUTHOR: Please provide the page range for reference [8].**	
7	**AUTHOR: Please provide the page range for reference [9].**	
8	**AUTHOR: Please provide the page range for reference [10].**	
9	**AUTHOR: Please provide the page range for reference [12].**	
10	**AUTHOR: Please provide the page range for reference [13].**	
11	**AUTHOR: Please provide the page range for reference [14].**	
12	**AUTHOR: Please provide the page range for reference [15].**	
13	**AUTHOR: Please provide the page range for reference [20].**	
14	**AUTHOR: Please provide the page range for reference [23].**	
15	**AUTHOR: Please provide the page range for reference [24].**	
16	**AUTHOR: Please provide the page range for reference [25].**	
17	**AUTHOR: Please confirm that given names (red) and surnames/family names (green) have been identified correctly.**	

Proof Correction Marks

Please correct and return your proofs using the proof correction marks below. For a more detailed look at using these marks please reference the most recent edition of The Chicago Manual of Style and visit them on the Web at: http://www.chicagomanualofstyle.org/home.html

Instruction to typesetter	*Textual mark*	*Marginal mark*
Leave unchanged	··· under matter to remain	stet
Insert in text the matter indicated in the margin	∧	∧ followed by new matter
Delete	through single character, rule or underline or through all characters to be deleted	
Substitute character or substitute part of one or more word(s)	through letter or through characters	new character ∤ or new characters ∤
Change to italics	— under matter to be changed	ital
Change to capitals	≡ under matter to be changed	caps
Change to small capitals	= under matter to be changed	sc
Change to bold type	~ under matter to be changed	bf
Change to bold italic	≈ under matter to be changed	bf+ital
Change to lower case	Ⱡ	lc
Insert superscript	∨	∨ under character e.g. ᵛ
Insert subscript	∧	∧ over character e.g. ₐ
Insert full stop	⊙	⊙
Insert comma	☆	☆
Insert single quotation marks	↓ ↓	↓ ↓
Insert double quotation marks	↓↓ ↓↓	↓↓ ↓↓
Insert hyphen	=	=
Start new paragraph	¶	¶
Transpose	⊔⊓	⊔⊓
Close up	linking ⁀ characters	⁀
Insert or substitute space between characters or words	#	#
Reduce space between characters or words	⌣	⌣